第 34 卷第 3 期 无 机 化 学 学 报 Vol.34 No.3
2018 年 3 月 CHINESE JOURNAL OF INORGANIC CHEMISTRY 579-588

水热合成 LuF_3:Yb^{3+},Er^{3+}微晶及其上转换发射与温度传感特性

王 祺 廖金生* 郭江飞 黄海平 温和瑞
(江西理工大学,冶金与化学工程学院,赣州 341000)

摘要: 通过在不同 pH 值下的简易水热法合成不同 Yb^{3+}离子($n_{Yb^{3+}}/n_{Lu^{3+}}$=5%~15%)和 Er^{3+}离子($n_{Er^{3+}}/n_{Lu^{3+}}$=1%~5%)掺杂浓度的 LuF_3:Yb^{3+},Er^{3+}微晶荧光粉。发现 pH 值对正交相 LuF_3:Yb^{3+},Er^{3+}的合成起着关键作用。在 980 nm 激发下,LuF_3:Yb^{3+},Er^{3+}荧光体呈现出以 523 nm($^2H_{11/2}\rightarrow{}^4I_{15/2}$)和 539 nm($^4S_{3/2}\rightarrow{}^4I_{15/2}$)为中心的强绿光上转换(UC)发射以及以 660 nm($^4F_{9/2}\rightarrow{}^4I_{15/2}$)为中心弱红光上转换发射。通过使用 X 射线衍射(XRD)和光致发光(PL)分析测定了最强发射强度的 Er^{3+}和 Yb^{3+}的最佳掺杂浓度。浓度依赖性研究表明,达到最强的绿光上转换发光时最佳掺杂浓度为 10%Yb^{3+},2%Er^{3+}。通过改变泵浦功率来研究 LuF_3:Yb^{3+},Er^{3+}荧光粉 UC 发光机制。通过 980 nm 二极管激光器在 293~573 K 的范围内研究了在 523 和 539 nm 处的 2 个绿光 UC 发射带的荧光强度比(FIR)的温度依赖性,发现在 490 K 得到最大灵敏度约为 15.3×10^{-4} K^{-1}。这表明 LuF_3:Yb^{3+},Er^{3+}荧光体可应用于具有高灵敏度的光学温度传感器。

关键词: 上转换; 稀土离子; 水热合成; 温度传感特性
中图分类号: O614.33 **文献标识码**: A **文章编号**: 1001-4861(2018)03-0579-10
DOI:10.11862/CJIC.2018.067

Upconversion Emission and Temperature Sensing Behavior of LuF_3:Yb^{3+},Er^{3+} Microcrystals Prepared by One-Step Hydrothermal Synthesis

WANG Qi LIAO Jin-Sheng* GUO Jiang-Fei HUANG Hai-Ping WEN He-Rui
(*School of Metallurgy and Chemical Engineering, Jiangxi University of Science and Technology, Ganzhou, Jiangxi* 341000, *China*)

Abstract: LuF_3:Yb^{3+},Er^{3+} microcrystals codoped with Yb^{3+} ($n_{Yb^{3+}}/n_{Lu^{3+}}$=5%~15%) and Er^{3+} ions ($n_{Er^{3+}}/n_{Lu^{3+}}$=1%~5%) were synthesized by a facile hydrothermal process at different pH values. It is found that the pH value has a crucial effect on synthesis of the orthorhombic phase LuF_3:Yb^{3+},Er^{3+}. Under 980 nm excitation, LuF_3:Yb^{3+},Er^{3+} phosphors exhibit strong green upconversion (UC) emission bands centered at 523 ($^2H_{11/2}\rightarrow{}^4I_{15/2}$) and 539 nm ($^4S_{3/2}\rightarrow{}^4I_{15/2}$) and weak red emissions near 660 nm ($^4F_{9/2}\rightarrow{}^4I_{15/2}$). The optimum doping concentrations of Er^{3+} and Yb^{3+} for the highest emission intensity were determined by using X-ray diffraction (XRD) and photoluminescence (PL) analyses. Concentration dependent studies reveal that the optimal composition is 10% Yb^{3+} and 2% Er^{3+} co-doping concentration with a strong green emission. A possible UC mechanism for LuF_3:Yb^{3+},Er^{3+} depends on the pump power is discussed. The temperature dependence of the fluorescence intensity ratios (FIR) for the two green UC emission bands peaked at 523 and 539 nm was studied in the range of 293~573 K under excitation by a 980 nm diode laser and the maximum sensitivity was approximately 15.3×10^{-4} K^{-1} at 490 K. This indicates that LuF_3:Yb^{3+}, Er^{3+} phosphors are potential candidates for optical temperature sensors with high sensitivity.

Keywords: upconversion; rare earth ions; hydrothermal synthesis; temperature sensing behavior

收稿日期:2017-09-28。收修改稿日期:2017-11-20。
国家自然科学基金(No.51162012)、江西省教育厅重点基金(No.GJJ160597)和江西省自然科学基金重大项目(No.20165ABC28010)资助。
*通信联系人。E-mail:jsliao1209@126.com

0 Introduction

Rare-earth (RE) ion doped luminescence upconversion (UC) materials have attracted much attention owing to their wide application prospects in solid-state lasers[1], luminescence display panels[2-3], solar cells[4-6], biological labels[7], biological imaging[8], and optical temperature sensors[9-10]. Recently, applying these UC materials as temperature sensing medium has attracted great attention[11-17]. In this application, the optical temperature sensors based on the fluorescence intensity ratio (FIR) technique as a noninvasive thermometry are considered to be an alternative candidate to replace traditional temperature sensors because they can be operated in some harsh environments such as electrical power stations, building fire detection, oil refineries. Furthermore, the FIR technique which takes the advantage of temperature dependence of two thermally coupled energy levels of RE ions, can reduce the dependence of measurement conditions and improve the sensitivity[18-19].

Erbium ion (Er^{3+}) has attracted much attention due to its unique electric energy level structures. The lifetimes of some intermediate energy levels of Er^{3+} are long enough. Thus, Er^{3+} ion is a promising competitor for UC luminescence center. Green UC luminescence of Er^{3+} ion hold a pair of thermally coupled emission levels ($^2H_{11/2}$ and $^4S_{3/2}$), whose emission intensity ratio would vary with environment temperature. It is well known that the $^2H_{11/2}\rightarrow{}^4I_{15/2}$ transition of Er^{3+} is hypersensitive, and the temperature sensitivity of the materials varies remarkably for Er^{3+} ions in different hosts[8-24]. Therefore, finding a host capable to provide suitable crystal field environment surrounding Er^{3+} dopant to enhance radiative probability of the $^2H_{11/2}\rightarrow{}^4I_{15/2}$ hypersensitive transition is a key for obtaining high temperature sensitivity of Er^{3+}.

Binary rare earth fluorides (REF_3) have been considered as an excellent luminescent rigid host matrix for various optically active lanthanide ions (Ln^{3+}), because they normally possess a high refractive index and low phonon energy (<400 cm^{-1}), which leads to the low probability of nonradiative decay and consequently the luminescence quantum yields are usually higher than in oxide hosts and in most inorganic matrixes. Recently, several chemical synthesis techniques to prepare Ln^{3+} doped REF_3 phosphors are available such as thermal decomposition[25], coprecipitation reaction[26], hydrothermal method[27]. Among all the methods for the synthesis of Ln^{3+} doped REF_3 phosphors, hydrothermal method has been proven to be an effective and convenient wet chemistry technique. During the hydrothermal process, chemical reactions are carried out under autogenous pressure and at temperatures above the boiling point of water in the autoclave[28]. Moreover, the size distribution of particles, phase compositions, and morphologies can be easily controlled by modifying the reaction conditions such as reaction temperature, pH value, and the starting materials. However, to the best of our knowledge, there is little or no investigation on the UC emission and temperature sensing performances of LuF_3:Yb^{3+}, Er^{3+} microcrystals prepared by hydrothermal method without any surfactant. We report here the hydrothermal synthesis of the Yb^{3+}/Er^{3+} co-doped LuF_3 microcrystals and determine how synthetic parameter can influence the textural and optical properties of the resulting UC materials. The luminescence properties of LuF_3:Yb^{3+},Er^{3+} microcrystals are investigated by changing doping concentrations of Yb^{3+} (and Er^{3+}) ions in the host. Additionally, their thermometry behaviors have also been illustrated by FIR technique.

1 Experimental

1.1 Sample preparation

All the chemicals of Lu_2O_3 (99.99%), Er_2O_3 (99.99%), Yb_2O_3 (99.99%), NaF (AR), HNO_3 and NaOH were used as the starting materials without any further purification. LuF_3:Yb^{3+},Er^{3+} samples for different Yb^{3+} doping concentration (5%~15%) with a fixed Er^{3+} concentration (2%) and Er^{3+} doping concentration (1%~5%) with a fixed Yb^{3+} concentration (10%) were prepared by the hydrothermal method without employing any surfactants. A typical procedure for the LuF_3:Yb^{3+},Er^{3+} (Yb10%, Er2%) sample synthesis as an example is described as follows: 0.350 2 g Lu_2O_3,

0.039 4 g Yb_2O_3 and 0.007 6 g Er_2O_3 were first dissolved in dilute nitric acid under heating. After the Lu_2O_3, Yb_2O_3 and Er_2O_3 were completely dissolved, the extra nitrite acid was removed by evaporation. Then deionized water was added to obtain $Lu(NO_3)_3$, $Yb(NO_3)_3$ and $Er(NO_3)_3$ mixed solution. Meanwhile 0.335 9 g NaF ($n_{RE(NO_3)_3}$:n_{NaF}=1:4) was dissolved in deionzed water while stirring. Second, the obtained NaF solution was slowly added into the above solution with magnetic stirring. Afterward the pH value of the solution was adjusted via using nitric acid or NaOH. The resultant milky colloidal suspension was transferred into a 100 mL Teflon-lined stainless-steel autoclave, sealed and heated to 180 ℃ for 21 h. Finally, the autoclave was cooled to room temperature naturally, and the products were deposited at the bottom of vessel. The precipitate was separated by centrifugation and washed three times with absolute alcohol. After being dried in air at 80 ℃ for 12 h, the final powder products were obtained. Other phosphor samples were prepared by the same procedure, except for changing $Ln(NO_3)_3$ and the pH value.

1.2 Characterization

X-ray diffractometer (XRD) patterns of samples were examined on a X′Pert PRO (PANalytical) powder diffractometer with Cu $K\alpha$ (λ=0.150 465 nm, 40 kV, 40 mA) radiation to identify the crystal phase. The XRD data within the range from 10° to 80° were recorded in a scanning mode with a step size of 0.02° and a step scanning time of 8 s for Rietveld refinement. The morphology of the samples was characterized by a JSM6700F scanning electron microscope (SEM) operated at 10 kV and a JEOL-2010 transmission electron microscope (TEM) equipped with the energy dispersive X-ray spectrum (EDS) operated at 200 kV. In order to investigate the temperature dependence of the UC emission, the sample was placed in a temperature-controlled copper cylinder, and its temperature was increased from 293 to 573 K. The UC spectra of sample at various temperatures were obtained using a Fluorolog-3 double monochromator equipped with a Hamamatsu R928 Photomultiplier under the excitation of a 980 nm diode laser with 150 mW (the power density is about 3 W·cm^{-2}).

2 Results and discussion

2.1 Effect of the pH for solution on the crystal structure

The crystallinity and phase purity of the as-prepared samples are examined with XRD. Fig.1 shows XRD patterns of the as-obtained samples at 180 ℃ for 21 h with different pH values in comparison to the standard card. As shown in Fig.1, it is obvious that all diffraction peaks of the product obtained at the mixed

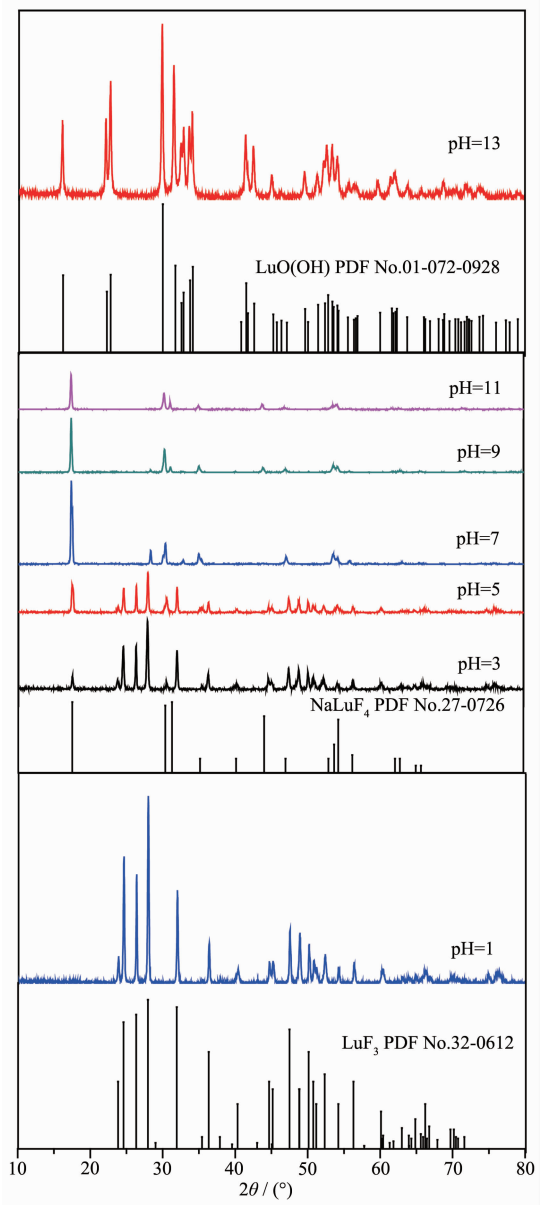

Fig.1　XRD patterns for as-obtained sample with different pH values; Standard data for LuF_3 (PDF No.32-0612) is also presented in the figure

solution of pH=1 could be clearly indexed to the pure orthorhombic phase LuF_3 (PDF No.32-0612). When the pH value of the mixed solution is 3, it is clearly seen that other impurity phase (hexagonal $NaLuF_4$ PDF No. 27-0726) emerged. With the pH value of the mixed solution continuing to increase to 7, it is clearly seen that $NaLuF_4$ is the main phase. With the pH value of the mixed solution increasing until 13, it is clearly seen that the diffraction peaks of the product matched well with the standard data of monoclinic LuO(OH) (PDF No.01-072-0928). The above-stated results indicate that the pH value is very important for preparing the pure orthorhombic phase LuF_3.

Rietveld refinement is an effective method to analyze the position of atoms in a primitive cell. In order to evaluate the structural parameters of LuF_3:10%Yb^{3+},2%Er^{3+}, structural refinement was carried out by the TOPAS (total pattern analysis solutions) program using the Rietveld method. Fig.2 gives the experimental and refined XRD patterns of the LuF_3:10%Yb^{3+},2%Er^{3+} sample. The black crosses and red solid line represent the experimental and calculated patterns, respectively. The pink vertical lines show the positions of the simulated diffraction patterns. The difference between the experimental and calculated results is plotted by the blue line at the bottom. By comparing the calculated data with the experimental

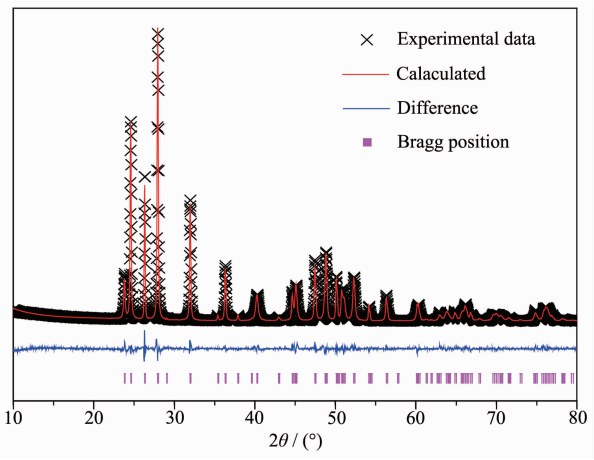

Fig.2 XRD refinement result for the LuF_3:10%Yb, 2%Er sample, showing the Bragg reflection positions, the observed and calculated XRD profiles, and the difference between the observed and calculated patterns

data, we find that each peak is in good agreement. There is no impurity phase found in the samples, which reveals that it is a good single phase. The Rietveld refinement analysis indicates the values (R_p= 5.28% and R_{wp}=6.77%, where R_p is the residual obtained by directly calculating the XRD spectrum calculated from the model structure and the experimental data and R_{wp} is the weight to specific position, which are within the accepted error range, indicating that the refinement results and the above assumption are reliable. According to the literature, the Yb^{3+} and Er^{3+} ions occupy the site of Lu^{3+} ions. In order to further evaluate the occupying sites of the doping ions of Yb^{3+} and Er^{3+}, structural refinement was also carried out on LuF_3:10%Yb^{3+},2%Er^{3+}, as shown in Fig.2. The resulting crystallographic data of LuF_3:10% Yb^{3+},2% Er^{3+} are summarized in Table 1. The atomic coordinates and site occupancy fraction (SOF) are presented in Table 2.

Table 1 Crystal structural data and lattice parameters for LuF_3:10%Yb, 2%Er

Formula	LuF_3:10%Yb, 2%Er
Space group	*Pnma*(No.62)
Symmetry	Orthorhombic
Formula weight	231.615 4
Z	4
a / nm	0.614 97
b / nm	0.677 08
c / nm	0.448 13
V / nm^3	0.186 595
R_p / %	5.28
R_{wp} / %	6.77

A low-magnification SEM image (Fig.3a) of the LuF_3:10% Yb^{3+},2% Er^{3+} sample shows that the morphology is octahedral-like structure with good uniformity and dispersity. Fig.3b a high magnification SEM image of the prepared powders. As can be seen in these images, the LuF_3:10%Yb^{3+},2%Er^{3+} sample show smooth and the particle size is about 4.5 μm. Morphological observation by transmission electron microscopy (TEM) is also shown in Fig.3c. The TEM image of the Yb^{3+}/Er^{3+} co-doped LuF_3 sample indicates the particle size is 4.5 μm, which accords well with the result of SEM. Combining with the high resolution

Table 2　Atomic coordinates and site occupancy fraction (SOF) for LuF_3:10%Yb, 2%Er

Atom	*x*	*y*	*z*	SOF
Lu	0.367 573	0.250 000	0.049 804	0.88
Yb	0.364 828	0.250 000	0.055 816	0.1
Er	0.361 028	0.250 000	0.057 762	0.02
F1	0.166 980	0.058 857	0.364 448	1
F2	0.024 045	0.250 000	0.899 741	1

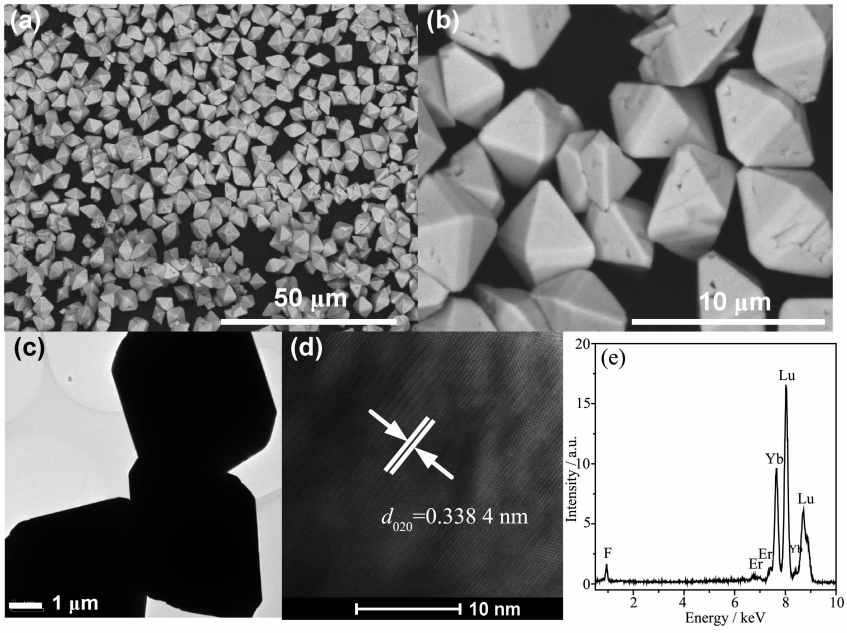

Fig.3　Low- (a) and high-magnification (b) SEM images of LuF_3:10%Yb^{3+}, 2%Er^{3+} sample; (c) TEM image of LuF_3:10%Yb^{3+}, 2%Er^{3+} sample; (d) HRTEM image of LuF_3:10%Yb^{3+}, 2%Er^{3+} sample; (e) EDS data taken from a single particle

TEM image (HRTEM) (Fig.3d), it can be clearly seen that the lattice fringes show the imaging characteristics in which the orthorhombic structure LuF_3 crystal where the interplanar spacing of 0.338 4 nm corresponds to the distance of the (020) plane. The EDS was used to further characterize the chemical composition of the as-prepared product, and the results shown in Fig.3e confirm that element ratios consist with the chemical formula of Yb^{3+}/Er^{3+} co-doped LuF_3 sample for 10%Yb^{3+} and 2%Er^{3+}, with n_{Yb}:n_{Er}:n_{Lu}=5∶1∶44. The results confirm that Yb^{3+} and Er^{3+} ions have been effectively incorporated into the LuF_3 host lattice, agreeing with the XRD analysis above. The above results indicate that the LuF_3:Yb^{3+},Er^{3+} micorcrystals can be successfully obtained by one-step hydrothermal method.

2.2　UC luminescence studies

To investigate influence of the synthesis parameter (pH value) on UC emission of as-obtained samples, the UC emission spectra of the as-obtained samples with different pH values are shown in Fig.4a. It is obvious that green and red UC emissions of the product obtained at the mixed solution of pH=1 is strongest among those of all pH values. When the pH value of the mixed solution is 3, it is clearly seen that UC emission obviously decrease and the relative intensity of green and red light is opposite compared with that of pH=1, which is due to other impurity phase ($NaLuF_4$) emerged. The other impurity phase leads to luminescence quenching. With the increase of the pH value of the mixed solution, UC emissions of the products continually decrease. The increase of the concentration of the other impurity will further lead to luminescence quenching. The above-stated results

indicate that the pH value as synthesis parameter is very important for obtaining strong UC emission.

In order to investigate concentration quenching of Yb^{3+}/Er^{3+} co-doped LuF_3, Fig.4b and 4c show the dependence of the UC luminescence spectra of the Yb^{3+}/Er^{3+} co-doped LuF_3 phosphors on the sensitizer (Yb^{3+}) and activator (Er^{3+}) concentrations, respectively. Intense green emission at 523 and 539 nm ($^2H_{11/2}\rightarrow{}^4I_{15/2}$ and $^4S_{3/2}\rightarrow{}^4I_{15/2}$ transitions of Er^{3+}) and weak red emission at 660 nm ($^4F_{9/2}\rightarrow{}^4I_{15/2}$ transition of Er^{3+}) are

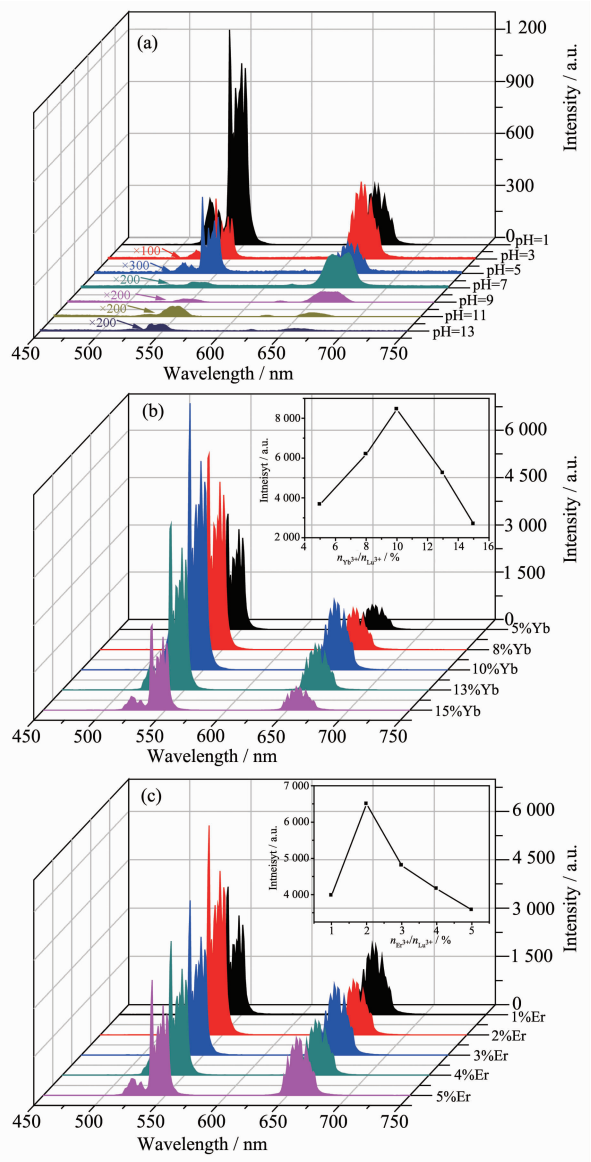

Fig.4 UC emission spectra of the LuF_3:Yb^{3+},Er^{3+} samples for (a) different pH values, (b) different Yb^{3+} concentrations with a fixed 2%Er^{3+} and different Er^{3+} concentrations with a fixed 10%Yb^{3+} (c) under 980 nm excitation

observed in the emission spectra. As the concentrations of Er^{3+} are fixed at 2%, the green emission intensity becomes stronger with the increasing of Yb^{3+} content and reaches a maximum at 10% in the range of 5%~15%, which is shown in Fig.4b. The concentration quenching effect appears in this system and results in intensity decreasing as the concentration of Yb^{3+} over 10%. This is believed to be due to the onset of the quenching effect that transfers the excitation of Er^{3+} back to Yb^{3+} and self-quenching in high-Yb^{3+} doping concentration[29-31]. As the concentrations of Yb^{3+} are fixed at 10%, the green emission intensity becomes stronger with the increasing of Er^{3+} content and reaches a maximum at 2% in the range of 1%~5% (Fig.4c). The concentration quenching effect is caused by the cross-relaxation process among Er^{3+} ions. The concentration quenching will not occur at low concentration, because the distance between identical Er^{3+} ions is so large that the energy migration is hampered[32]. With the increase of the Er^{3+} concentration, the average distance between Er^{3+} ions become shorter and the energy transfer become convenient. The critical distance of which can prevent the energy transfer happening can be calculated by the following formula[33]: $R_c=2[3V/(4\pi NX_c)]^{1/3}$, where V is the volume of the unit cell, X_c is the critical concentration and N is the number of available crystallographic sites occupied by the activator ions in the unit cell. The values of V and N for the crystalline LuF_3 (orthorhombic system, a=0.614 97 nm, b=0.677 08 nm, c=0.448 13 nm, Z=4, $V=abc$, $N=Z$) are 0.186 595 nm^3 and 4, respectively. Considering the above optimum concentration as the critical concentration X_c, the R_c for Er^{3+} is 1.645 4 nm in the LuF_3:10%Yb^{3+},2%Er^{3+} phosphors.

In order to investigate the UC mechanism, pump power-dependence of green and red UC emission spectra in LuF_3:Yb^{3+},Er^{3+} micorcrystals was measured and displayed in a logarithmic scale (Fig.5). The emission intensity I_{em} depends on the excitation power I_P following to the relationship of $I_{em}\propto I_P^n$, where n is the number of the pumping laser photons required to excite RE ions from the ground state to the emitting excited state. The slopes (n) of the linear fittings are

1.75 for green emission ($^2H_{11/2}\rightarrow{}^4I_{15/2}$ and $^4S_{3/2}\rightarrow{}^4I_{15/2}$) and 1.90 for red emission ($^4F_{9/2}\rightarrow{}^4I_{15/2}$), indicating that two-photon processes are required to populate the $^2H_{11/2}$, $^4S_{3/2}$ and $^4F_{9/2}$ emitting levels, respectively.

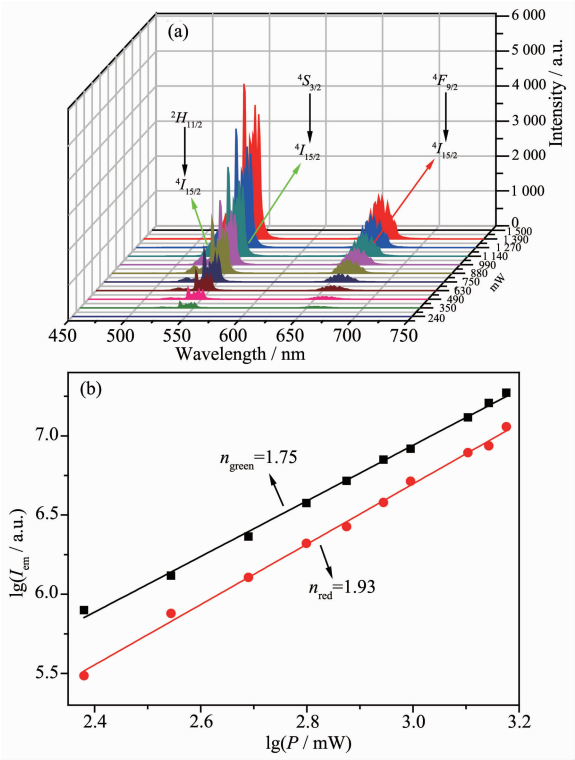

P is the pump power values

Fig.5　(a) UC spectra of LuF_3:Yb^{3+},Er^{3+} phosphors for different laser powers of 980 nm excitation; (b) Dependences of the UC intensities (I_{em}) of green ($^2H_{11/2}$, $^4S_{3/2}$)$\rightarrow{}^4I_{15/2}$ and red $^4F_{9/2}\rightarrow{}^4I_{15/2}$ transitions on the 980 nm pumping laser power (I_p) for LuF_3:Yb^{3+},Er^{3+} phosphors

Fig.6 displays the energy levels of Yb^{3+} and Er^{3+} ions in LuF_3:Yb^{3+},Er^{3+} micorcrystals aswell as the proposed UC mechanisms. As for Yb^{3+}/Er^{3+} codoped system under 980 nm excitation, the 980 nm laser photon excites the Yb^{3+} ion from the $^2F_{7/2}$ ground state to the $^2F_{5/2}$ excited state. And the excited Yb^{3+} ion in the $^2F_{5/2}$ state transfers it excitation energy to one nearby Er^{3+} ion. The Er^{3+} ion at the ground $^4I_{15/2}$ state is excited to the upper $^4F_{7/2}$ state via two energy transfer (ET_1 and ET_2) processes[34]. Subsequently, the non-radiative relaxation process of $^4F_{7/2}$ state populates two lower energy levels ($^2H_{11/2}$ and $^4S_{3/2}$), resulting in the green ($^2H_{11/2}\rightarrow{}^4I_{15/2}$ and $^4S_{3/2}\rightarrow{}^4I_{15/2}$) UC emissions. The weak red UC emission centered at 660 nm is originated from $^4F_{9/2}\rightarrow{}^4I_{15/2}$ transition. There exist two main possible pumping mechanisms for red emission. The first pumping mechanism is the nonradiative relaxation from the populated $^4S_{3/2}$ state to the $^4F_{9/2}$ state through multphonon interaction. In the second pumping mechanism, Er^{3+} ion can be relaxed from $^4I_{11/2}$ level to $^4I_{13/2}$ level, and then excited to $^4F_{9/2}$ state via ET_3 process.

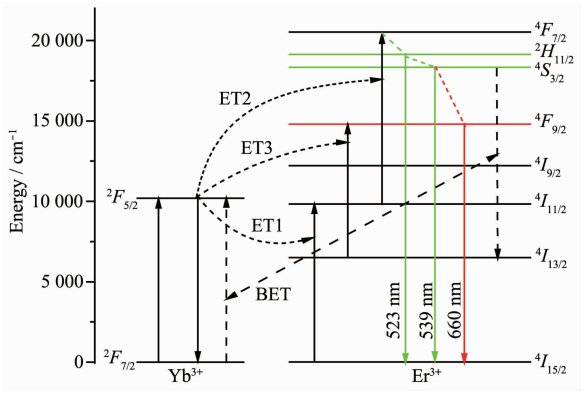

ET stands for energy transfer

Fig.6　Energy level diagrams of Yb^{3+} and Er^{3+} ions and UC emission mechanism in LuF_3:Yb^{3+}, Er^{3+} phosphors

2.3　Effect of temperature on UC emission and temperature-sensing behavior

As already mentioned, UC bands centered at 523 and 539 nm arise from $^2H_{11/2}\rightarrow{}^4I_{15/2}$ and $^4S_{3/2}\rightarrow{}^4I_{15/2}$ transitions. The energy gap between the levels $^2H_{11/2}$ and $^4S_{3/2}$ of Er^{3+} is around 568 cm^{-1}, the state of $^2H_{11/2}$ may also be populated from $^4S_{3/2}$ by thermal excitation and the UC emission intensity ratio of emission band at 523 to 539 nm could change with the variable temperature, therefore it is could be used as optically temperature sensor for the present UC phosphors. In order to investigate the temperature sensing properties of as-prepared phosphors, the green UC emission spectra for LuF_3:10%Yb^{3+},2%Er^{3+} phosphor at various temperature (from 293 to 573 K) are presented in Fig. 7, in which the spectra are normalized to the emission peak at 539 nm. It is found that no remarkable shift in emission wavelength for the sample while the fluorescence intensity ratio (FIR) of UC emission from $^2H_{11/2}\rightarrow{}^4I_{15/2}$ to $^4S_{3/2}\rightarrow{}^4I_{15/2}$ increases with the rise of

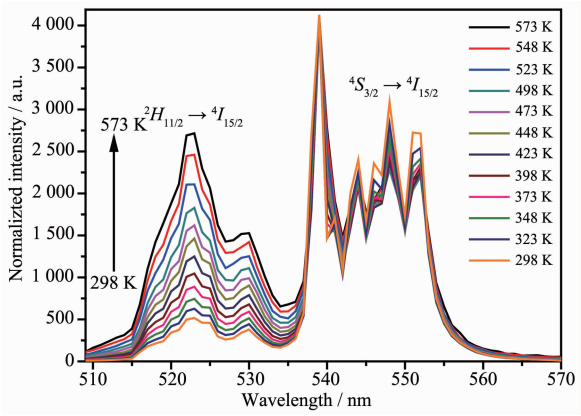

Spectra are normalized to the emission peak at 539 nm; Excitation power density is 3 W·cm^{-2}

Fig.7 Temperature dependence of the green UC luminescence spectra of LuF_3:Yb^{3+}, Er^{3+} phosphor under 980 nm excitation

temperature. The relative population of the thermally coupled energy levels follows the Boltzmann distribution and the FIR of two emissions can be written as follows[35]:

$$FIR=I_H/I_S=[g_H\omega_H\delta_H/(g_S\omega_S\delta_S)]\exp[-\Delta E/(kT)]=B\exp[-\Delta E/(kT)] \quad (1)$$

where I_H and I_S are intensities (the integrated areas below the emission curves) for the upper ($^2H_{11/2}\rightarrow{}^4I_{15/2}$) and lower ($^4S_{3/2}\rightarrow{}^4I_{15/2}$) thermally coupled levels transitions, respectively. In general, N, g, ω, δ represent the number of ions, the degeneracy, the angular frequency, the emission cross section of fluorescence transitions from excited state ($^2H_{11/2}$ and $^4S_{3/2}$) to the ground state ($^4I_{15/2}$), respectively. ΔE is the energy gap between the $^2H_{11/2}$ and $^4S_{3/2}$ levels, k is the Boltzmann constant, and T is the absolute temperature. B is the pre-exponential factor.

The fluorescent intensity ratio (FIR) of these two UC emissions shows a remarkable dependence on the temperature (Fig.8a). According to the expression of the FIR, the value of Ln(FIR) versus the inverse absolute temperature (1/T) is plotted in Fig.8b. The linear fitting of the experimental data gave slope and intercept equal to 980.69 and 1.02, respectively. As a consequence, the energy gap ΔE and the pre-exponential constant are evaluated to be about 680 cm^{-1} and 2.77, respectively. These two parameters are vital factors for the sensitivity (S) of temperature detection, as defined by the following equation[35]:

$$S=\mathrm{d}FIR/\mathrm{d}T=FIR[\Delta E/(kT^2)]=B[\Delta E/(kT^2)]\exp[-\Delta E/(kT)] \quad (2)$$

where the term FIR is the symbol used for fluorescence intensity ratio. The calculated values of sensor sensitivity were plotted as a function of absolute temperature (Fig.8c) and found to be maximum about 15.3×10^{-4} K^{-1} at 490 K. The temperature sensitivity of LuF_3:Yb^{3+}, Er^{3+} phosphor is comparable to that (15.7×10^{-4} K^{-1} at

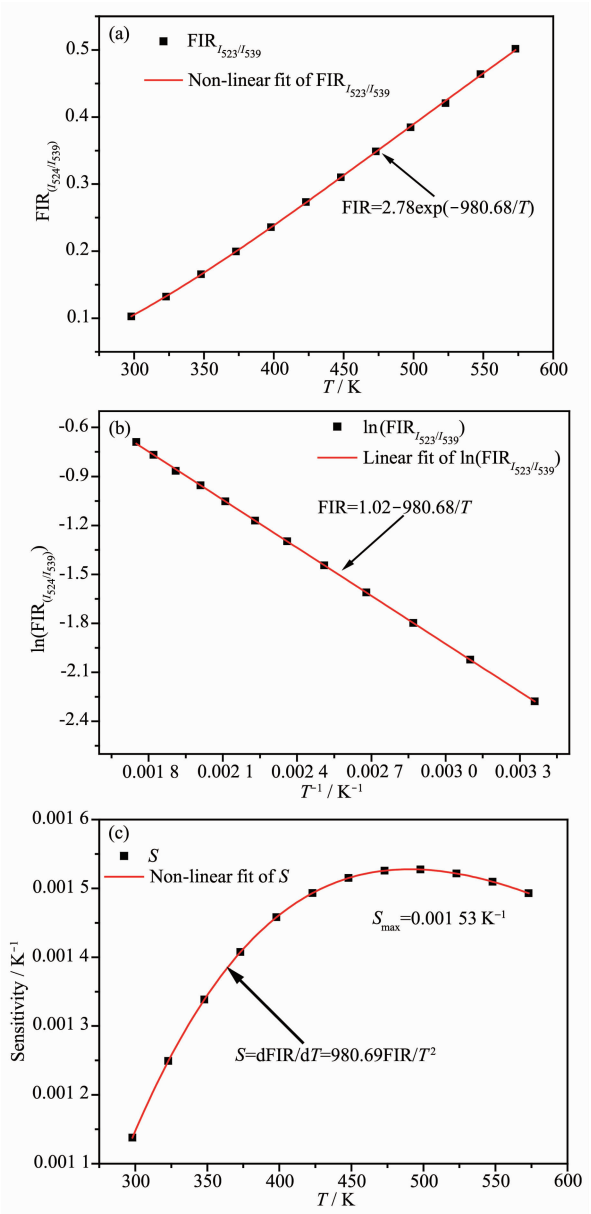

Fig.8 Upconversion-based temperature-sensing behaviour of LuF_3:Yb^{3+}, Er^{3+} phosphor: (a) FIR relative to the temperature; (b) Monolog plot of the FIR as a function of the inverse absolute temperature; (c) Sensor sensitivity as a function of temperature

386 K) of LaF_3:Yb^{3+}/Er^{3+} phosphor[36]. Therefore, the Yb^{3+}/Er^{3+} co-doped LuF_3 micorcrystals can be used as an efficient optical temperature sensor.

3 Conclusions

In summary, the LuF_3:Yb^{3+},Er^{3+} microcrystals have been prepared by one-step hydrothermal method at 180 ℃ for 21 h under pH=1. The intense visible UC luminescence of sample is clearly observed under 980 nm excitation. The mechanisms of UC lumine-scence and the changes of the emission intensity with Yb^{3+} concentration or Er^{3+} concentration are discussed. The transition mechanisms of the UC luminescence can be ascribed to a two-photon absorption process. The best doping concentration of LuF_3 for UC emission is about 10%Yb^{3+} and 2%Er^{3+}. The green UC emission bands observed around 523 ($^2H_{11/2}\rightarrow{}^4I_{15/2}$) and 539 nm ($^4S_{3/2}\rightarrow{}^4I_{15/2}$) have been utilized for optical thermometry via the fluorescence intensity ratio technique. The dependence of FIR for the sample LuF_3:10%Yb^{3+},2%Er^{3+} with optimal composition on temperature were measured in the range of 293~573 K, and the sensitivities of sample reach the maximum 15.3×10^{-4} K^{-1} at 490 K. All these results suggest that Yb^{3+}/Er^{3+} co-doped LuF_3 phosphor materials can be explored UC fluorescence imaging and temperature measurements with high sensitivity.

Acknowledgements: This work was financially supported by the National Natural Science Foundation of China (Grant No. 51162012), the Science Program of the Education Office, Jiangxi Province (Grant No.GJJ160597) and the Major Project of Natural Science Foundation of Jiangxi Province (Grant No. 20165ABC28010).

References:

[1] Auzel F. *Chem. Rev.*, **2004**,**104**:139-173

[2] Downing E, Hesselink L, Ralston J, et al. *Science*, **1996**,**273**: 1185-1189

[3] Binnemans K. *Chem. Rev.*, **2007**,**107**:2592-2614

[4] Cheng Y Y, Nattestad A, Schulze T F, et al. *Chem. Sci.*, **2016**,**7**:559-568

[5] LI Shu-Quan(李树全), LIN Jian-Ming(林建明), WU Ji-Huai (吴季怀), et al. *Chinese J. Inorg. Chem.*(无机化学学报), **2009**,**25**:60-64

[6] LIAO Jin-Sheng(廖金生), SU Zhen-Yu(苏振欲), ZHOU Dan (周单), et al. *Chinese J. Inorg. Chem.*(无机化学学报), **2013**, **29**:2351-2356

[7] Chen Z G, Chen H L, Hu H. *J. Am. Chem. Soc.*, **2008**,**130**: 3023-3029

[8] Shang L, Dong S J, Nienhaus G U. *Nano Today*, **2011**,**6**:401-418

[9] DU Xin-Chao(杜新超), HE Zhen-Quan(贺正权), LIN Xiao (林霄), et al. *Acta Photonica Sin.*(光子学报), **2015**,**44**: 406003-406009

[10]Zuo Q H, Luo L H, Yao Y J. *J. Alloys Compd.*, **2015**,**632**: 711-716

[11]Bao Y N, Xu X S, Wu J L, et al. *Ceram. Int.*, **2016**,**42**: 12525-12530

[12]Li X P, Wang X, Zhong H, et al. *Ceram. Int.*, **2016**,**42**: 14710-14715

[13]Marciniak L, Waszniewska K, Bednarkiewicz A, et al. *J. Phys. Chem. C*, **2016**,**120**:8877-8882

[14]Ananias D, Paz F, Yufit D, et al. *J. Am. Chem. Soc.*, **2015**, **137**:3051-3058

[15]Marciniak L, Prorok K, Francés-Soriano L, et al. *Nanoscale*, **2016**,**8**:5037-5042

[16]Marciniak L, Bednarkiewicz A, Hreniak D, et al. *J. Mater. Chem. C*, **2016**,**4**:11284-11290

[17]Vetrone F, Naccache R, Zamarron A, et al. *ACS Nano*, **2010**,**4**:3254-3258

[18]Soni A K, Rai V K, Kumar S. *Sens. Actuators B*, **2016**,**229**: 476-482

[19]Yang X X, Fu Z L, Yang Y M, et al. *J. Am. Ceram. Soc.*, **2015**,**98**:2595-2600

[20]Dong B, Cao B S, Feng Z Q, et al. *Sens. Actuators, B*, **2012**, **165**:34-37

[21]Singh S K, Kumar K, Rai S B. *Sens. Actuators, A*, **2009**, **149**:16-20

[22]Singh A K, Shahi P K, Rai S B, et al. *RSC Adv.*, **2015**,**5**: 16067-16073

[23]Ding M Y, Chen D Q, Lu C H, et al. *Mater. Lett.*, **2017**,**189**: 5-8

[24]Suo H, Zhao X Q, Zhang Z Y, et al. *Chem. Eng. J.*, **2017**, **313**:65-73

[25]Sun X, Zhang Y W, Du Y P, et al. *Chem. Eur. J.*, **2007**,**13**: 2320-2332

[26]Singh A K, Kumar K, Pandey A C, et al. *Spectrochim. Acta, Part A*, **2013**,**106**:236-241

[27]Wang X, Zhuang J, Peng Q, et al. *Inorg. Chem.*, **2006**,**45**: 6661-6665

[28]Yan B, Wu J H. *J. Mater. Res.*, **2009**,**24**:3050-3056

[29]Hinojosa S, Meneses-Nava M A, Barbosa-Garcia O, et al. *J. Lumin.*, **2003**,**102**:694-698
[30]Auzel F, Baldacchini G, Laversenne L, et al. *Opt. Mater.*, **2003**,**24**:103-109
[31]Zhu H Y, Lin M, Jin G R, et al. *J. Lumin.*, **2017**,**851**:292-297
[32]Guo C F, Ding X, Seoc H J, et al. *J. Alloys Compd.*, **2011**, **509**:4871-4874
[33]Blasse G. *Philips Res. Rep.*, **1969**,**24**:131-44
[34]Shi L S, Shen Q Y, Qiu Z Z. *J. Lumin.*, **2014**,**148**:94-97
[35]Dong B, Cao B S, He Y Y. *Adv. Mater.*, **2012**,**24**:1987-1993
[36]Cheng X R, Ma X C, Zhang H J, et al. *Physica B*, **2017**, **521**:270-274